Uncertainty quantification of the lifetime of self-healing thermal barrier coatings based on surrogate modelling of thermal cyclic fracture and healing

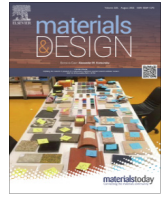Kumthekar, Anuj; Ponnusami, Sathiskumar A.; van der Zwaag, Sybrand; Turteltaub, Sergio

Important note
To cite this publication, please use the final published version (if applicable).
Please check the document version above.

Uncertainty quantification of the lifetime of self-healing thermal barrier coatings based on surrogate modelling of thermal cyclic fracture and healing

Anuj Kumthekar [a], Sathiskumar A. Ponnusami [b], Sybrand van der Zwaag [a], Sergio Turteltaub [a,*]

[a] Faculty of Aerospace Engineering, Delft University of Technology, Kluyverweg 1, 2629 HS Delft, the Netherlands
[b] Department of Mechanical Engineering and Aeronautics, City, University of London, Northampton Square, EC1V 0HB London, United Kingdom

HIGHLIGHTS

- Uncertainty Quantification of TBC lifetime can be described using polynomial chaos.
- The sensitivity analysis identifies the most efficient self-healing material system.
- The interface amplitude is the most significant contributor of TBC lifetime variance.
- Healing particles improves TBC lifetime but leads to increased scatter in fatigue.
- Self-healing variables act in a coupled manner on crack growth rate variance.

GRAPHICAL ABSTRACT
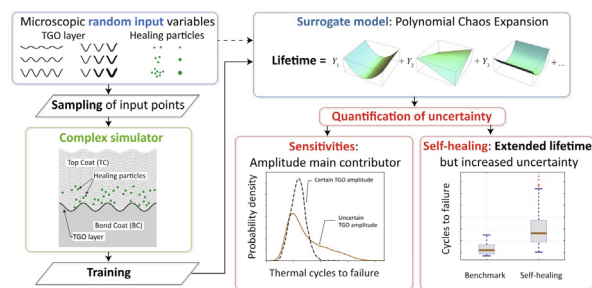
ABSTRACT

Computationally-efficient surrogate models based on a Polynomial Chaos Expansion (PCE) are developed to quantify the uncertainties in the fracture behavior and lifetime of a self-healing thermal barrier coating system (SH-TBC) and a benchmark conventional TBC system. The surrogate models are built using deterministic information from micromechanical finite element simulations of thermal cycling of the systems, which are conducted until failure by spallation. Fracture and healing events are simulated using a cohesive-zone based crack healing model. The thermally-grown oxide layer (TGO) interface amplitude and its growth rate, the diameter and volume fraction of healing particles, and the mean distance of particles from the interface are used as training variables. Statistical characteristics and sensitivity indices are obtained from the trained models. It is found that the interface amplitude is the most significant contributor to the variance in the TBC lifetime, with other parameters displaying a relatively minor influence. Healing particles extend the expected value of TBC lifetime, however they also increase the uncertainty of thermal fatigue life. The analysis of self-healing TBCs exemplifies how PCE-based surrogate models can serve as a powerful tool for deriving design insights in complex material systems.

© 2022 The Author(s). Published by Elsevier Ltd. This is an open access article under the CC BY license (http://creativecommons.org/licenses/by/4.0/).

---

* Corresponding author.
E-mail addresses: A.Kumthekar@student.tudelft.nl (A. Kumthekar), Sathiskumar.Ponnusami@city.ac.uk (S.A. Ponnusami), S.vanderZwaag@tudelft.nl (S. van der Zwaag), S.R.Turteltaub@tudelft.nl (S. Turteltaub).

1. Introduction

Thermal barrier coatings (TBC) are thermal insulation layered systems applied in high temperature environments in order to protect the underlying structural substrate from oxidation and thermal degradation while enabling a higher operating temperature range and thus higher thermodynamic efficiency [1]. In the aerospace industry, TBCs play a prominent role since it is the most commonly used process to protect jet turbine blades. Consequently, the safety and integrity of the turbines as well as maintenance and reparation schedules strongly depend on the lifetime of these coating systems.

A cross-section of a barrier coating manufactured by air-plasma spray is shown in Fig. 1. The top side is exposed to a high-temperature environment and the substrate that needs to be protected is located at the bottom (not shown in the figure). This TBC system is composed of a metallic bond coat (BC) layer and a top coat (TC) layer which is made up of a ceramic material. High temperature diffusion of oxygen through the top coat leads to oxidation with the metal-rich bond coat and the formation of a thin thermally grown oxide (TGO) layer at the TC/BC interface. During thermal cycling, stresses are generated within the TBC due to a mismatch in the thermomechanical properties of the individual layers as well as the growth of TGO layer which lead to development of microcracks [1,2]. With the progression of thermal cycles, these microcracks can grow and coalesce, eventually causing spallation, which exposes the underlying substrate to extreme temperatures. As a result, the TBC lifetime is measured by the number of thermal cycles that the TBC can sustain until spallation. In order to arrest the cracks and potentially improve the TBC lifetime, researchers have investigated the implementation of self-healing particles within the coatings [3–6]. One of the most widely studied methods of incorporating self-healing properties in a TBC is to include encapsulated healing agents within the top coat, which is the location where cracks typically appear in TBCs (see Fig. 1). Once activated by a growing microcrack, they initiate a chemical reaction which fills the crack and restores the mechanical integrity.

Finite element simulations have been extensively used to study the influence of self-healing particles and other microstructural parameters on the TBC lifetime [7–18]. These numerical simulation techniques can in general capture the experimentally-observed damage process that occurs in metallo-ceramic material systems [19,20]. However, finite element methods are deterministic in nat-ure, neglecting the randomness in the output as a result of possible uncertainties in the inputs. These uncertainties can arise due to partial or incomplete knowledge about the process, structure or properties of the system which is being simulated. Propagating these input uncertainties through the system helps to quantify the uncertainty in the output, hence promoting robust designing. This can be achieved with the help of an *uncertainty quantification* framework. This framework can be utilized to quantify the uncertainties in input variables using stochastic calibration with the existing data, which is then followed by quantifying the uncertainty propagation in the output quantities [21].

One commonly-used approach towards *uncertainty propagation* is Monte Carlo sampling. This is a random sampling technique that involves evaluating a deterministic computational model at points that are sampled from the input variable distributions in order to obtain the output distribution. However, Monte Carlo sampling is ineffective in practical terms due to the requirement of large sample size and hence the computational costs for achieving space-filling characteristics within the input variable space [22]. In order to circumvent this issue, *surrogate modelling* can be utilized. Surrogate modelling (or metamodeling) is a technique in which a computationally inexpensive model is developed which approximates the predictions of the original model with the help of a limited number of sample evaluations [23]. One of the widely used meta-models is *polynomial chaos expansion* (PCE) [24] in which the variation in the output or the quantity of interest is represented using orthogonal polynomials in uncertain input variables. Surrogate modelling approaches have been applied for the design of composites [25–27] as well as the study of crack growth [28,29].

Self-healing TBC systems are defined by various material and geometric parameters that are inherently uncertain in nature. Further, owing to the expensive computational costs associated with lifetime predictions of such TBC systems, Monte Carlo sampling and similar techniques are currently not feasible from a practical point of view. In this context, the present work aims to develop a surrogate model that approximates the self-healing TBC micromechanical model for evaluation of TBC lifetime and the determination of sensitivity to microstructural parameters. This information can be used for a robust material design of self-healing thermal barrier coatings.

The work is organized as follows: Section 2 reports the details of the PCE model and the implemented framework for training the surrogate model. The deterministic model for a self-healing TBC system is summarized in Section 3, which includes the modeling details of the self-healing TBC unit cell along with a description of the utilized micromechanical model. The SH-TBC trained surrogate model, the supporting discussion, and the model validation process have been described in Section 4. Section 5 includes two extensions for the use of surrogate models, namely a surrogate model for the benchmark system (conventional TBC without healing particles) and a surrogate model for crack growth (instead of lifetime). A comparison between the SH-TBC and benchmark TBC responses is made in order to determine whether the use of self-healing particles helps to improve the expected value of TBC lifetime. The surrogate model for crack growth rate is used to elucidate the uncertainty in the damage *process* instead of the accumulated damage itself. Finally, Section 6 provides the conclusion and recommendations based on the obtained results.

2. Surrogate model for the lifetime of a self healing thermal barrier coating system

2.1. Background

For the present work, the particle-based self healing thermal barrier coating system presented in [5] is used as the main tem-

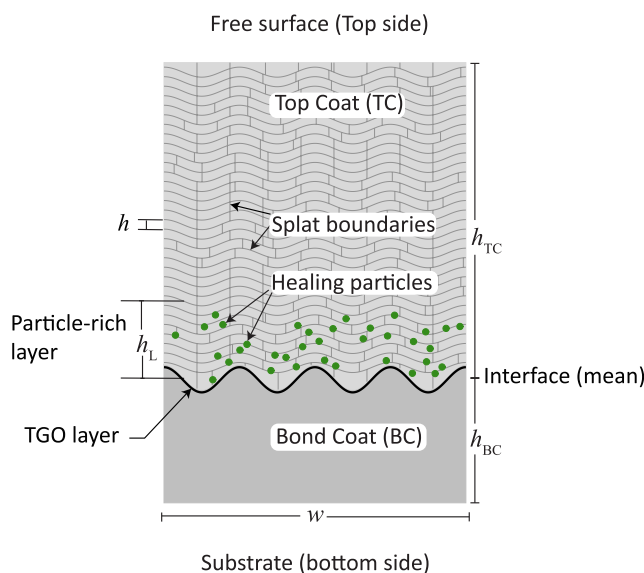Free surface (Top side)

Substrate (bottom side)

Fig. 1. Unit cell for the self-healing TBC system.

plate to generate a surrogate model for its lifetime. This is due to the fact that the corresponding computational framework was developed to simulate the complete thermal cycling evolution of the material system until failure, thus allowing to predict its lifetime. However, it is relevant to mention that the methodology presented here for the surrogate model can be applied for the lifetime of other material systems or to establish surrogate models for other quantities of interest with suitable modifications.

The uncertain input variables that are taken into account for the lifetime are essentially of two types:

(a) Microstructural features that have been previously identified, either experimentally and/or through simulations, as likely to have a strong influence in the lifetime of a TBC system and
(b) Design parameters for a *self-healing* TBC that are not easily controllable during manufacturing or that can vary between a given design range.

In the first category, the roughness of the TC/BC interface and the growth rate of TGO layer are taken as uncertain input variables. For the second type, the volume fraction of the healing particles in the top coat layer, the diameter of the healing particles and their mean distance from the TC/BC interface have been chosen as uncertain input variables. All other model parameters, including material properties, are taken as deterministic values. In principle it is possible to include more uncertain variables in the analysis but the associated computational costs of each new input random variable may be significant. Correspondingly, the choice of uncertain input variables is taken as a compromise between incorporating previous experience in the analysis while providing enough flexibility to the simulation framework to discover previously unknown relations. The following subsections describe the key ingredients of the computational framework and discuss the procedure in the development of the surrogate model in detail.

2.2. Uncertainty propagation using polynomial chaos expansion

Consider an uncertainty characterized by an output random variable Y that depends on input random variables collected in a vector $\boldsymbol{\phi} = (\phi_1, \ldots, \phi_K)$, with K being the number of input variables. Polynomial chaos expansion is a stochastic approach in which Y can be represented as an infinite series expansion of orthogonal polynomials $\psi_i, (i = 0, \ldots, \infty)$ that form a basis with respect to the joint probability density function of the input variables $\boldsymbol{\phi}$. In turn, the polynomials ψ_i are obtained by carrying out a tensor product of univariate orthogonal polynomials $P_j, (j = 1, \ldots, K)$ [30,24]. Correspondingly, the random variable Y can be represented as

$$Y = \sum_{i=0}^{\infty} y_i \psi_i(\boldsymbol{\phi}) \qquad \text{with} \qquad \psi_i(\boldsymbol{\phi}) = \prod_{j=1}^{K} P_j^{\alpha_j^i}(\phi_j), \qquad (1)$$

where y_i are the representation coefficients of Y and α_j^i corresponds to the order of the univariate orthogonal polynomial P_j for the orthogonal polynomial ψ_i (e.g., Hermite polynomials for normally distributed random variables or Legendre polynomials for uniformly distributed random variables).

The series expansion given in (1) is often truncated to a polynomial of finite order n since the response of the system converges after a certain number of terms and consideration of additional terms does not make any notable contribution towards the system response [26]. Hence, the truncated expansion $\widehat{Y} \approx Y$ can be expressed as

$$\widehat{Y} = \sum_{i=0}^{Q-1} \hat{y}_i \psi_i(\boldsymbol{\phi}) \qquad \text{with} \qquad Q = \frac{(K+n)!}{K!n!} \quad \text{and} \quad 0 \leqslant \sum_{j=1}^{K} \alpha_j^i \leqslant n, \tag{2}$$

thus the polynomial expansion is approximated with Q terms, which is a function of the number of input random variables K and the maximum order of the expansion n.

A simple surrogate model $\widehat{Y}$ for a random variable Y can be obtained by specifying the coefficients $\hat{y}_i, (i = 0, \ldots, Q-1)$, in the truncated polynomial chaos expansion given in (2). This can be done by calibrating the coefficients $\hat{y}_i$ with the help of responses from the original model at selected sample points from the space of input variables. In the present context, the random variable Y of interest is the SH-TBC lifetime and the original model refers to a detailed finite-element simulation of the healing and damage process due to thermal cycling until failure by spallation, which provides the lifetime measured as the number of cycles until failure. The detailed finite element simulation, including cracking and healing constitutive models, corresponds in the present work to the so-called *complex simulator*.

Generally, the techniques used to compute the coefficients $\hat{y}_i$ are divided into two classes: intrusive and non-intrusive methods. Intrusive methods involve modification of the original finite element code in which residual minimization has to be carried out in the weak form of the mathematical model or the utilization of the Galerkin approach. This weak form can be generated by projecting the original model on the polynomial chaos basis function [31]. The inelastic nature of the problem at hand creates a challenge in terms of using intrusive methods. Alternatively, the non-intrusive methods do not require alteration in the original deterministic finite element code and this approach is adopted in the sequel.

A commonly-used non-intrusive technique is the least squares approximation or the point collocation approach in order to train the PCE surrogate model [22]. In this approach, the original model needs to be evaluated for a number N of sampled points from the space of the input variables. The sampled points $\boldsymbol{\phi}^{(j)}, (j = 1, \ldots, N)$, are transformed to their corresponding standard distributions $\boldsymbol{\gamma}^{(j)}$ (e.g., symmetric, zero mean and unit standard deviation for a normal distribution), and the original model is used to compute the values of $Y(\boldsymbol{\gamma}^{(j)})$ for each data point j. Subsequently, the sum S of squares of residuals between the outputs of the original model and the approximated PCE representation given in (2) is calculated as [25]

$$S = \sum_{j=1}^{N} \left(Y(\boldsymbol{\gamma}^{(j)}) - \sum_{i=0}^{Q-1} \hat{y}_i \psi_i(\boldsymbol{\gamma}^{(j)}) \right)^2. \tag{3}$$

Equating the partial derivative of the residual with respect to each of the coefficients to zero and solving the resulting system of linear equations provides the required coefficients, i.e.,

$$\frac{\partial S}{\partial \hat{y}_i} = 0 \qquad i = 0, 1, \ldots, Q-1. \tag{4}$$

Correspondingly, the training process requires a design of experiments (or design of simulations in the present case) for the generation of the trained data set. To this end, a Latin Hypercube Sampling approach is chosen [32]. This quasi-random technique is commonly used since it requires a relatively small number of sample points for covering the input space as compared with other sampling techniques. As shown in the next section, the total number of sample points is chosen as a compromise between the accuracy and variance of the surrogate model and the associated computational cost [33]. The overall workflow to develop a PCE-based surrogate model is summarized in Fig. 2.
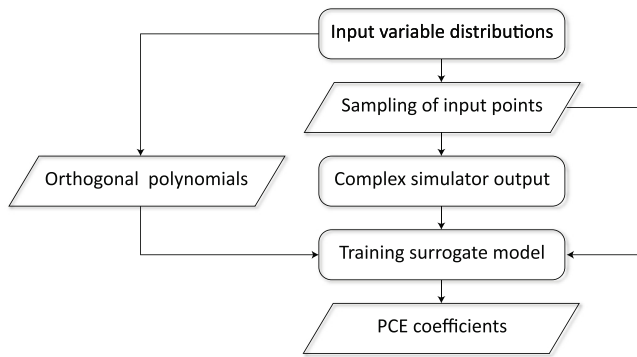
Fig. 2. Framework to develop the PCE surrogate model.

2.3. Definition of input variable uncertainties

As indicated above, the output random variable of interest is the TBC lifetime subjected to thermal cycling and the uncertain input variables that are considered are (i) the TC/BC interface amplitude, (ii) the TGO growth rate, (iii) the volume fraction of the healing particles, (iv) the diameter of the healing particles and (v) the mean distance of the healing particles from the TC/BC interface. The joint probability distribution can be derived by defining the individual input variable distributions, which in turn can be decided based on experimental observations, existing information and expert understanding [34].

The morphology of the TC/BC interface, where eventually the TGO appears and grows during thermal cycling, is known to have a significant influence on the TBC lifetime. As illustrated in Fig. 1, this interface is often modeled using a sinusoidal shape with a given amplitude. In order to observe the influence of the TC/BC interface morphology on the TBC lifetime, a uniform distribution of values of the interface amplitude A is considered within the range $[A_{min}, A_{max}]$, with $A_{min} = 15\,\mu m$ and $A_{max} = 25\,\mu m$. This representative range is chosen based on experimental observations and finite element simulations [35–37]. For the second input variable considered, a logarithmic function is utilized to fit the experimentally observed TGO growth curves that indicate the TGO thicknesses h_{TGO} as a function of number of thermal cycles $m \geqslant 1$, with

$$h_{TGO} = c \ln m \qquad (5)$$

where the coefficient c allows to quantify the TGO growth rate for a given thermal cycle (see [5,38]). Accordingly, the variation in TGO growth rate has been quantified with the assumption that c varies uniformly in the range $[c_{min}, c_{max}]$, with $c_{min} = 2.5\,\mu m$ and $c_{max} = 3\,\mu m$. As explained in more detail below, this distribution has been identified with the help of prior simulations, which were carried out for a range of TGO growth rate coefficient values in order to determine the viability of duration of simulations for the available computational resources. Observe that, in principle, it is also possible to model the TGO growth based on a coupled diffusion–reaction process, see e.g., [39,40]. However, for the purposes of the present analysis, it is more convenient to directly impose the growth rate from experimentally-observed curves since this allows to directly establish the influence of this parameter on the system's lifetime.

In the simulations, the healing particles are embedded in a sub-layer of the TC, located close to the TC/BC interface. This critical sub-layer is prone to development of cracks due to a mismatch of thermomechanical properties of individual layers, which is aggravated by the growth of the TGO between the TC and BC layers during thermal cycling. The volume fraction ξ of healing particles within this sub-layer, measured in percentage as the ratio between the volume occupied by the particles and the volume of the sublayer, is represented using a normal (Gaussian) distribution with a mean value of 7.5% and a standard deviation of 1%. In this case, the normal distribution represents uncertainty in the manufacturing of a self-healing system with a given design volume fraction that was previously chosen based on a parametric analysis. The diameter of the healing particles is assumed to be characterized by a uniform distribution in the range $[d_{min}, d_{max}]$, with $d_{min} = 10\,\mu m$ and $d_{max} = 20\,\mu m$. These are representative values for (encapsulated) healing particles that have been previously proposed and manufactured. A uniform distribution is chosen instead of, for example, a normal distribution, in order to represent distinct design choices. Similarly, the value for the mean distance of healing particles from the TC/BC interface has been distributed uniformly between $[l_{min}, l_{max}]$, with $l_{min} = 45\,\mu m$ and $l_{max} = 80\,\mu m$. These values are chosen such that the healing particles encompass a range of possible designs of sub-layers concentrated close to the TC/BC interface covering the considered range of volume fraction and diameter of healing particles. The input variable uncertainties have been summarized in Table 1.

2.4. Selecting the Polynomial Chaos Expansion order and the number of sample points

The first step to obtain the orthogonal polynomials for the joint probability distribution of the input parameters is to select the order of the PCE. It has been observed that there are no specific guidelines to set a particular order since the optimum order may vary in different underlying models [25]. In general, a choice can be made for (i) the total number of sample points N, (ii) the number of random variables K used as input for the PCE and (iii) the maximum order of the polynomial n with the goal of reaching a compromise between the accuracy and variance of the surrogate model and the associated computational cost. The number of sample points N is related to the number of coefficients Q in the truncated PCE (2) through the so-called oversampling ratio $n_p = N/Q$. As a guideline, it has been suggested to use an oversampling ratio $n_p = 2$, which provides an idea of the required number of sample points N for a given number of input random variables K and PCE order n [41]. In view of (2), the number of sample points N required with the suggested oversampling ratio $n_p = 2$ is shown in Table 2. Each sample point corresponds to a computationally expensive simulation. For example, running a simulation with the computational model used in [5] with 10 processors in a cluster takes an average execution time of 60 h (not including pre and post-processing). As a result, for the present work, a PCE order $n = 2$ has been chosen such that, in combination with the chosen number of input random variables $K = 5$ and the oversampling ratio $n_p = 2$, it requires $N = 42$ simulations. The chosen quadratic order satisfies current computational constraints and is also able to capture the possible non-linearities in the response of the underlying

Table 1
Statistical characteristics of random input variables.

Input	Description	Distribution	Parameters
A	Interface amplitude	Uniform	$A_{min} = 15\,\mu m$ $A_{max} = 25\,\mu m.$
c	TGO growth coefficient	Uniform	$c_{min} = 2.5\,\mu m$ $c_{max} = 3\,\mu m$
ξ	Volume fraction healing particles	Normal	Mean: 7.5 %, std dev = 1 %
d	Diameter healing particles	Uniform	$d_{min} = 10\,\mu m$ $d_{max} = 20\,\mu m$
l	Mean distance from interface	Uniform	$l_{min} = 45\,\mu m$ $l_{max} = 80\,\mu m$

Table 2
Number of sample points N with PCE order n and number of input variables K for an oversampling ratio $n_p = 2$. For the present work, the combination $K = 5$ and $n = 2$ was chosen, resulting in $N = 42$ sample points.

	K					
n	1	2	3	4	5	6
1	4	6	8	10	12	14
2	6	12	20	30	42	56
3	8	20	40	70	112	168

model as well as the interactions between the input variables. It has also been observed in the literature that a second-order PCE is able to demonstrate sufficient accuracy in determining the mean and standard deviation of the response, whereas a higher order might be required in order to accurately determine higher order statistical moments such as skewness and kurtosis [42]. Once the input variable uncertainties are defined in terms of their distributions, they can be utilized to obtain the orthogonal polynomials that will be used in the surrogate model. Simultaneously, as shown in the workflow in Fig. 2, a Latin Hypercube scheme is used to select the sample input points from the input variable space. These sampled points are utilized as inputs to the underlying complex simulator (see Section 3), the corresponding outputs of which are used to train the surrogate model (i.e., finding the coefficients $\hat{y}_i$ in (2)). In the present work, the implementation of the PCE workflow is done using the Python-based toolbox *Chaospy* [43]. Relevant details of the micromechanical model used to generate the data points are given in the next section.

3. Complex simulator

3.1. TBC micromechanical finite element analysis

The self-healing TBC micromechanical model developed in [5] has been utilized in order to obtain the number of cycles to TBC failure as a consequence of exposure to thermal cyclic behavior. Most of the applications of TBCs involve a typical thermal loading cycle consisting of three distinct phases: heating, dwelling and cooling. To this end, the simulation framework considers a heating phase in which the temperature is increased from 30°C (nominal ambient temperature) to 1100°C (test temperature). This is followed by the dwelling phase in which the TBC is exposed to constant elevated temperature of 1100°C. Finally, the cooling process involves reduction of temperature from 1100°C to 30°C. It has been assumed that during the dwelling phase, the TBC system does not experience any thermomechanical stresses since the elevated temperature is considered to be the coating deposition temperature. Consequently, the cooling phase is responsible for the generation of thermomechanical stresses due to the mismatch in thermal expansion coefficients between different components of the TBC system.

Fig. 1 describes a representative unit cell for the self-healing TBC micromechanical domain, which repeats itself horizontally along the substrate surface. A two-dimensional framework has been utilized to model the unit cell under plane strain condition during thermal cycling. It consists of separate constitutive models for the thermoelastic and fracture behavior of the ceramic top coat, metallic bond coat, thermally grown oxide layer at the TC/BC interface, the self-healing particles and the splat boundaries in the top coat that are characteristic of Air Plasma Sprayed (APS) TBCs. The roughness of the interface as well as the splat boundaries have been modeled in the form of sinusoidal curves. Typical samples subjected to thermal cycling in an oven are made of a substrate material coated with TBC to mimic the operating conditions. In the present work, only the coating is modeled and the influence

of the substrate and the testing conditions are reproduced with suitable boundary conditions. In particular, referred to a coordinate system with the origin taken at the bottom-left corner of the unit cell shown in Fig. 1 and with horizontal x and vertical y components, the traction components t_x and t_y on the top (T) edge are taken as zero (traction-free surface). Further, the effect of the substrate is taken into account assuming that the thermoelastic deformation of the substrate during thermal cycling is imposed on the relatively thin TBC layer at the bottom (B). Finally, lateral periodic boundary conditions are based on an assumption of an infinitely long coated surface by imposing compatible conditions for u_x and u_y displacement components, at the left (L) and right (R) edges of the unit cell. In view of these assumptions, the boundary conditions are as follows:

$$
\begin{aligned}
&t_x^T(x, H) = t_y^T(x, H) = 0 \\
&u_x^B(x, 0) = (1 + \nu_{\text{sub}})\alpha_{\text{sub}}\Delta T x + u_x^B(0, 0) \\
&u_y^B(x, 0) = 0 \\
&u_x^R(w, y) - u_x^L(0, y) = (1 + \nu_{\text{sub}})\alpha_{\text{sub}}\Delta T w \\
&u_y^R(w, y) - u_y^L(0, y) = 0
\end{aligned}
\tag{6}
$$

where ν_{sub} and α_{sub} represent, respectively, Poisson's ratio and the coefficient of thermal expansion values for the substrate, ΔT is the change in temperature during thermal cycling, w is the width of the unit cell and H its total height. The horizontal displacement $u_x^B(0, 0)$ of the origin of coordinates may be arbitrarily chosen and it is taken as zero. Thermal equilibrium is assumed during thermal cycling (quasi-static process), hence a uniform temperature is imposed in the whole unit cell, which evolves according to the imposed heating, dwelling and cooling times. The problem therefore consists on finding mechanical equilibrium in a quasi-static process taking into account cracking and healing as well as the growth of the TGO layer due to oxidation.

Representative values have been assigned to the geometrical features in the unit cell, where $h_{\text{TC}} = 500\,\mu m$, $h_{\text{BC}} = 200\,\mu m$ and $h = 15\,\mu m$ indicate the thicknesses of the TC, BC and the splats respectively whereas the wavelength of the sinusoidal interface curve has been assigned the value of $60\,\mu m$. The healing particles have been assumed to be distributed near the TC/BC interface within a layer of thickness $h_{\text{HL}} = 150\,\mu m$. The lengths of the splats have been set in such a way that the overall aspect ratio is representative of an APS-manufactured TBC [5,35]. A domain convergence analysis has been carried out for different values of TBC width $w = 240, 360, 480, 600, 720\,\mu m$. It has been observed that the change in the width normalized total crack size at failure is within 10% for the last three values considered ($w = 480, 600, 720\,\mu m$). Hence the TBC width has been assigned the value $w = 480\,\mu m$ for the rest of the analyses.

The computational framework involves a combination of separate modules using MATLAB and GMSH [44] to generate the geometry and the mesh (including cohesive elements that are inserted on all edges of bulk elements) and to assign the loading and boundary conditions as well as the material properties to different element sets. Inserting cohesive elements throughout the whole TBC domain ensures that the crack initiation and propagation is not biased by the presence or absence of cohesive elements in specific regions of the TBC domain. An input file is subsequently created to execute a finite element simulation in ABAQUS. The region near the TC/BC interface encompassing the healing particles has been discretized with a fine mesh having a characteristic size of $1\,\mu$m. This is because of the thermomechanical mismatch in properties near the TC/BC interface and the presence of healing particles that cause stress redistribution and eventually pave the way for initiation and propagation of cracks. On the other hand, in order to reduce the computational expense, the rest of the TBC domain has been dis-

cretized with a coarser mesh having a size of $2\,\mu$m. In the present work, the same material properties are used as in [5], including elastic and fracture characteristics of the TC, BC, TGO, healing particles, splats and interfaces. For detailed information regarding the utilized material properties, the reader is referred to [5].

3.2. Cracking and healing model

In order to describe the system behavior in response to cracking and subsequent healing, the cohesive zone based self-healing model developed by Ponnusami et al. [45] has been utilized. This model is based on a bilinear traction-separation law that takes as inputs the mode-I fracture energy and the normal fracture strength of the cohesive element material. The incorporation of self-healing and recovery of fracture properties is simulated with the help of a composite-based constitutive model in which the overall normal (n) and tangential (s) components of the traction $\tilde{t}$ are described as a weighted sum of the traction components of the original material and the healing material as follows:

$$\tilde{t}_n = w^{(0)}t_n^{(0)} + w^{(1)}t_n^{(1)} \qquad \tilde{t}_s = w^{(0)}t_s^{(0)} + w^{(1)}t_s^{(1)} \qquad (7)$$

where the superscripts 0 and 1 represent the original and healing materials, respectively and the weighting factors $w^{(0)}$ and $w^{(1)}$ can be interpreted as the surface-based volume fractions of the original and healing material, respectively, at the moment of activation of healing. In this context, volume fraction refers to the fraction of the crack area occupied by a material per unit crack opening displacement. In a two-dimensional setting, the crack area fraction refers to the crack length fraction per unit depth. The relation given in (7) is used after the first healing event occuring at time t^* in conjunction with an equivalent crack opening $\Delta^{(p)}$ for each material ($p = 0$ original material or $p = 1$ healing material), with

$$\Delta^{(p)} := \sqrt{\left\langle \delta_n - \delta_n^{(p)*} \right\rangle^2 + \gamma^2 \left(\delta_s - \delta_s^{(p)*}\right)^2}, \quad t \geqslant t^*, \qquad (8)$$

where γ is a parameter that controls the relative contribution from the normal and tangential openings on the effective crack opening for material p, $\delta_n^{(p)*}$ and $\delta_s^{(p)*}$ respectively measure the normal and tangential shift in the zero opening for the cohesive relation due to healing. In (8), the symbol $\langle \cdot \rangle = (\cdot + |\cdot|)/2$ refers to the Macauley bracket.

The crack opening or closing conditions are monitored with the loading function $f\left(\Delta^{(p)}, \kappa^{(p)}\right) = \Delta^{(p)} - \kappa^{(p)}$, where $\kappa^{(p)}$ is the damage history variable and corresponds to the maximum crack opening displacement throughout the loading history. The model further employs the classical Karush–Kuhn–Tucker relations for crack loading and crack unloading, from which an equivalent traction $T^{(p)}$ can be computed for the crack loading case using a linear degradation relation $T^{(p)} = \sigma^{(p)}\left(\Delta_f^{(p)} - \Delta^{(p)}\right)/\left(\Delta_f^{(p)} - \Delta_i^{(p)}\right)$, with $\Delta_i^{(p)}$ and $\Delta_f^{(p)}$ representing the initial and final (fully-cracked) crack-opening displacements. The crack unloading case follows a linear relation from $\Delta^{(p)} = \kappa^{(p)}$ to zero. Finally, the normal and tangential components required in (7) are computed consistent with the work equivalency relation $\tilde{t} \cdot \tilde{\delta} = T\Delta$, with $\tilde{\delta}$ being effective the crack opening vector.

An important advantage of the proposed model is the ability to simulate multiple and successive cracking and healing events with possibly multiple healing materials $p > 1$. The model has been incorporated into the framework of the simulation in the form of an ABAQUS user-material subroutine (UMAT). For more details regarding the process of identifying failed or fractured elements and the implementation of healing mechanism, see [45].

3.3. Simulation of oxide layer growth

In order to protect the substrate against oxidation, TBC systems usually have a controlled oxidation process in which the oxygen diffusing inwards from the high temperature free surface reacts with sacrificial aluminum in the metallic bond coating, forming oxides such as alumina and thus preventing the oxygen from actually reaching the substrate [5,46,47]. The drawback from this oxidation protection system is that the thermally grown oxide layer at the TC/BC interface generates significant thermal stresses during cycling due to the mismatch in stiffness and coefficients of thermal expansion. Since the lifetime of a TBC system strongly depends on damage triggered by thermal stresses, it is critical to include this phenomenon in the finite element analysis.

In order to simulate the growth of the TGO layer and its effects as a function of number of thermal cycles, a simplified TGO layer growth framework has been utilized in the ABAQUS UMAT. Experimentally determined isothermal TGO growth depicting the thickness of the TGO as a function of number of thermal cycles [38,48] have been utilized and the data have been fitted to the logarithmic function (5), which can be used in the subroutine in order to determine the TGO layer thickness as a function of number of thermal cycles. This curve fit is based on the assumption that most of the TGO growth occurs isothermally during the dwelling phase. This process has been simulated in the finite element model by an incremental replacement of the bond coat thermomechanical properties with those of the TGO material as a function of number of thermal cycles. This implies a presence of a mixture zone at the interface of the newly formed TGO layer and the existing BC layer as illustrated in Fig. 3 The properties of the material within the mixture zone have been assigned with the help of a weighted average of the constitutive properties of the pure TGO and BC materials, i.e., for any thermoelastic property f, it is evaluated as

$$f_{\text{mix}}(y, m) = \omega f_{\text{TGO}} + (1 - \omega)f_{\text{BC}} \qquad (9)$$

with

$$\omega(y, m) = \begin{cases} 0 & y > h_{\text{TGO}}(m) + h_{\text{mix}} \\ 1 & y \leqslant h_{\text{TGO}}(m) \\ \frac{y - h_{\text{TGO}}}{h_{\text{mix}}} & h_{\text{TGO}}(m) < y < h_{\text{TGO}}(m) + h_{\text{mix}} \end{cases} \qquad (10)$$

where $\omega = \omega(y, m)$ indicates the local fraction of TGO material in the mixture zone, h_{mix} is the thickness of the mixture zone, y is the normal distance from a point in the mixture zone to the location of the original TC/BC interface (before oxidation) and m indicates the number of thermal cycles. During the simulations of thermal
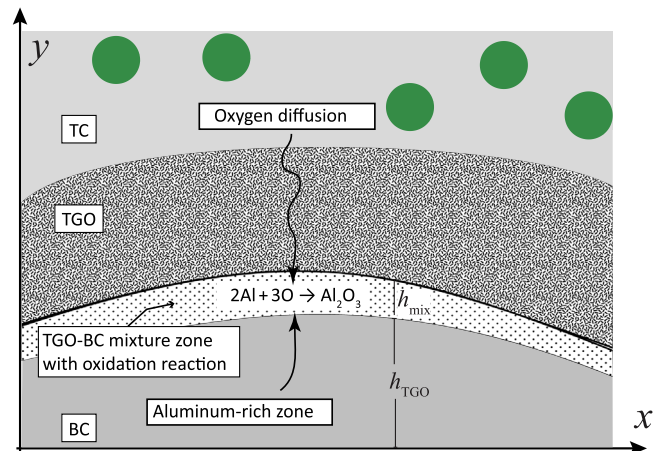

Fig. 3. TGO growth model in TC/BC interface.

cycling, the original computational domain is kept the same as shown in Fig. 1 but the region in the bond coat immediately adjacent to the TC/BC interface is updated after every cycle by combining (5) and (9). Effectively this allows to simulate the growth of the TGO layer in the FEM analysis.

3.4. Artificially accelerated thermal cycling

Experimental results of thermal cycling of TBC systems for the conditions stated in Section 3.1 indicate that in general the lifetime is of the order of several hundred thermal cycles, which is computationally expensive to simulate with the chosen model. In order to alleviate the overall computational cost while capturing the cyclic damage and healing, an artificially accelerated TGO growth has been considered, where one simulated cycle represents the TGO growth of β actual cycles. Hence, denoting as $\tilde{m}$ the number of computational cycles, then $m = \beta\tilde{m}$, where m represents the number of actual cycles. The assumption behind this approach is that the accumulated damage and healing during β cycles can be captured as the damage and healing of a single cycle. In principle this assumption contradicts the nature of inelastic processes that are path-dependent (i.e., cyclic damage and healing is not equivalent to a single damage event followed by a single healing event). However, due to the relatively slow growth of the TGO layer per actual cycle, it is implicitly assumed that during β cycles it is possible to represent the accumulated damage and healing since they occur at approximately the same loading conditions. The path-dependent nature of the process is then captured in larger increments of β cycles.

To implement this artificially accelerated thermal cycling, the growth model given in (5) is replaced by

$$h_{\text{TGO}} = \tilde{c}\ln\tilde{m} \qquad \tilde{c} = \frac{c\ln(\beta\tilde{m})}{\ln\tilde{m}}, \tag{11}$$

thus, despite the use of an accelerated growth, the same growth rate parameter c was used as input as indicated in Section 2.3. Based on previous numerical experimentation, the acceleration factor was chosen as $\beta = 25$, which is seen as a reasonable compromise between an approximation error and the corresponding computational benefit. Complete failure of the TBC system is considered to have taken place when 90% of the TC layer has separated from the TC/BC interface or the TGO layer. For conciseness, detailed results of the simulations are not shown here but the reader is referred to [5] for examples of similar (but distinct) results.

4. Uncertainty quantification of self-healing TBC lifetime

4.1. The trained surrogate model

The number of *computational* thermal cycles until failure is considered as the quantity of interest while training the PCE surrogate model. As indicated in the workflow in Fig. 2, the training data can be used to find the coefficients of the orthogonal polynomials derived from the Wiener–Askey scheme of polynomials [49,50]. Based on the aforementioned data, the resulting surrogate model $L_{\text{SH-TBC}}$ for the lifetime of a self-healing thermal barrier coating is given by

$$\begin{aligned} L_{\text{SH-TBC}} = {}& 470.53 - 38.14A + 0.53A^2 + 4.78Ac - 0.46A\xi + 0.27Ad - 0.01Al \\ & + 13.73c - 1.56c^2 - 9.63c\xi - 3.75cd + 0.01cl \\ & + 23.44\xi + 0.79\xi^2 + 0.12\xi d - 0.01\xi l \\ & - 8.02d + 0.27d^2 + 0.05dl - 1.19l + 0.01l^2 \end{aligned} \tag{12}$$

where $L_{\text{SH-TBC}}$ measures the computational thermal cycles until failure, which are scaled by a factor β from the actual thermal cycles (see Section 3.4). As indicated in Section 2.3, the input random variables are the TGO interface amplitude A, the TGO growth coefficient c, the volume fraction ξ of healing particles, the diameter d of the healing particles and the mean distance l of the healing particles to the TC/BC interface. The ranges for the random input variables in (12) are summarized in Table 1.

Due to its simplicity, the surrogate model given in (12) can be used in conjunction with Monte Carlo sampling in order to derive the probability density function of the self-healing TBC lifetime. It can also be used to observe the relative impact of each of the input variables on the variation in the output or the sensitivity indices. Additionally, after determination of the most sensitive input variables, the surrogate model can be helpful to obtain the statistical characteristics of the variation of TBC lifetime as a function of the sensitive variable while the uncertainties in the remaining variables are propagated through the surrogate model. This approach helps in the determination of the reliability of the surrogate model output in the form of standard deviations. However, before extracting information from the surrogate model, its quality and validity needs to be assessed.

4.2. Residual plot

To determine the validity of the actual data points and to have an indication regarding the goodness of fit, a residual plot is presented in Fig. 4a along with a plot of the actual model values against the surrogate model responses in Fig. 4b. In the residual plot, the horizontal axis consists of the actual data points (computational thermal cycles until failure) whereas the corresponding vertical axis indicate the residual between the actual values and those produced by the surrogate model.

The results shown in the figures illustrate the goodness of fit and, equally important, that the variation in the output can be explained by the input variables as the residual data points are scattered randomly around the zero line, which supports the validity of the trained model (i.e., there is no observable trend or non-randomness in the residuals [51,52]).

Additionally, the goodness of fit can also be quantified with the help of the coefficient of determination R^2, which can be computed for given sample points $\gamma^{(j)}$, $(j = 1, \ldots, N)$ as

$$R^2 = 1 - \frac{e_{\text{train}}}{\widehat{V}} \qquad \text{with} \qquad e_{\text{train}} = \frac{S}{N}, \tag{13}$$

where, e_{train} is the training error, S is the sum of the squares of the residuals given by (3) and $\widehat{V}$ represents the variance observed in the responses of the trained surrogate model [53].

However, as the cardinality or the number Q of terms in the PCE increases, the number of sampled points N also increases, which can lead to overfitting of the model to the actual data points. This phenomenon can lead to increased prediction errors while using the surrogate model on new data. In order to take this into account, the coefficient of determination can be modified and adjusted to the number Q of PCE coefficients as follows [25]:

$$R_A^2 = 1 - \left(\frac{N-1}{N-Q-1}\right)\left(1 - R^2\right). \tag{14}$$

Based on the $N = 42$ data points used in the present analysis, the trained surrogate model was such that $R^2 = 0.97$ and $R_A^2 = 0.94$. From these values, it can be observed that, despite the underlying complexities and non-linearities in the self-healing TBC model, the surrogate model is able to fit well to the actual data points.
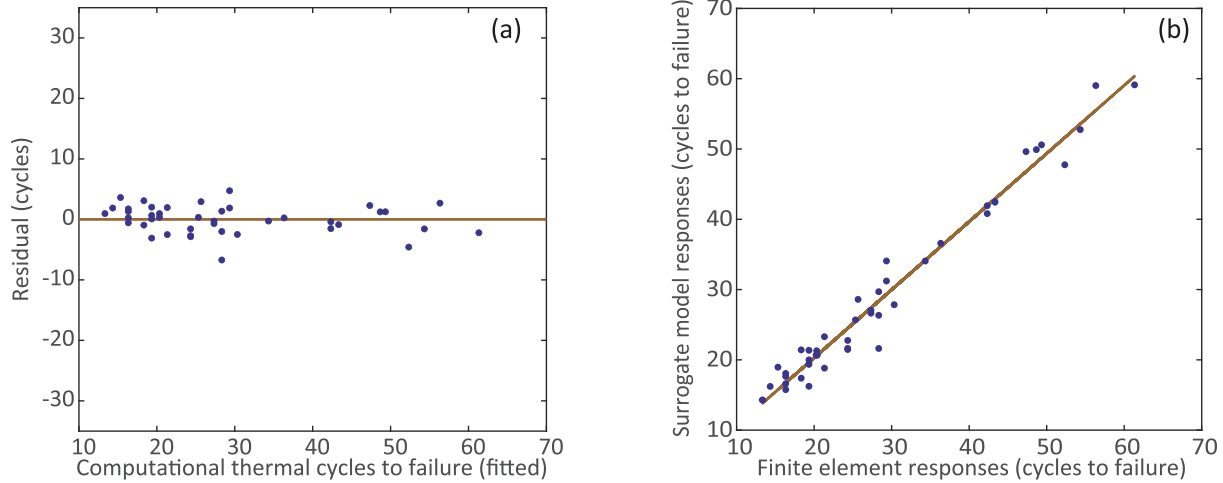
Fig. 4. Visualizing the goodness of fit for TBC lifetime prediction: (a): Residual plot and (b): surrogate model responses vs. complex simulator responses.

However, it has been observed that the adjusted coefficient of determination overpredicts the accuracy of approximation [54]. As a caveat, it is also relevant to mention that the evaluation of residuals and the goodness of fit does not indicate how well the trained model will perform on new data or unseen sample points.

4.3. Leave-one-out cross validation

The *leave-one-out* cross validation technique has been implemented to validate the trained model and determine its predictive performance. To this end, a collection of N surrogate models $\widehat{Y}^{(\sim i)}$ are built by training them on all but the ith sample point. Each metamodel is then used to predict the value of the original model Y at the ith observation and the prediction error is evaluated, i.e.,

$$\Delta^{(i)} = Y(\gamma^{(i)}) - \widehat{Y}^{(\sim i)}(\gamma^{(i)}). \tag{15}$$

This process is repeated for all the sample points and the predicted residual sum of squares or the leave-one-out cross validation error is calculated as [53]

$$e_{\text{L}} = \frac{1}{N} \sum_{i=1}^{N} \left(\Delta^{(i)} \right)^2. \tag{16}$$

Furthermore, in order to observe how the PCE order n affects the predictive performance of the surrogate model, the leave-one-out error of the current model that uses second order, $\widehat{Y} = \widehat{Y}_{n=2}$, has been compared with that of a model $\widehat{Y}_{n=1}$ developed using a PCE of first order. Using the same training data, the leave-one-out errors are $e_{\text{L}}\left(\widehat{Y}_{n=2}\right) = 28$ and $e_{\text{L}}\left(\widehat{Y}_{n=1}\right) = 41$, which confirms that the order $n = 2$ demonstrates a better predictive performance than the one developed with a PCE of order $n = 1$.

4.4. Sensitivity Analysis

In order to obtain the relative contribution of each input variable to the output variance, a sensitivity analysis can be carried out using the trained surrogate model. A commonly utilized approach to evaluate sensitivity indices is Sobol's method. Using this method, the output variance is decomposed into contributions associated with each of the input variables. For the random output variable Y that is a function of input variables $\boldsymbol{\phi} = (\phi_1, \phi_2, \ldots, \phi_K)$ the method to calculate the sensitivity index of ϕ_i is to initially fix the variable at a particular value $\phi_i = q_i$ and then calculating

the change in output variance or the conditional variance $V_{\phi_{\sim i}}(Y|\phi_i = q_i)$, which is computed considering the uncertainties in all but the ith input variable. Since ϕ_i also depicts uncertainty in terms of a distribution of values, a mean of the above-mentioned conditional variance is evaluated over the distribution of ϕ_i in order to obtain the expected value, i.e., $E[V_{\phi_{\sim i}}(Y|\phi_i)]$. The first order sensitivity index D_i of ϕ_i is given as

$$D_i = \frac{V(E_{\phi_{\sim i}}[Y|\phi_i])}{V(Y)} = 1 - \frac{E[V_{\phi_{\sim i}}(Y|\phi_i)]}{V(Y)} \tag{17}$$

where $V(Y)$ is the variance of the output variable and the alternative expression of D_i on the right hand side of (17) is obtained from the law of total variance. The first order sensitivity D_i is representative of the influence on the output variance of each input variable taken alone [42]. It is also convenient to determine the total sensitivity indices D_i^T, which include the possible interactions of input variables and hence their joint effect towards the output variance. The total sensitivity indices are given as

$$D_i^T = \frac{E_{\phi_{\sim i}}[V_{\phi_i}(Y|\phi_{\sim i})]}{V(Y)}. \tag{18}$$

The first-order and total sensitivities of the random input variables used in the surrogate model were computed using the Chaospy module in Python and are shown in Fig. 5a.

It can be observed that the TC/BC interface amplitude is the main contributor towards the variance in TBC lifetime. This implies that relatively small changes in the value of the amplitude will result in a high change in the TBC lifetime. In contrast, the uncertainty in the TGO growth coefficient has a lesser but still significant influence on the lifetime variance. Regarding the uncertainty of the design parameters for healing particles, the variation in particle diameter appears to be the most important within the range considered in Table 1, whereas the uncertainty in the volume fraction around the nominal value (mean) and the uncertainty in the deposition of healing particles (mean distance from particles to interface) have a low sensitivity.

In order to quantify how the output variance depends on the input variable sensitivity, two scenarios have been compared. The first one considers the uncertainties in all the input variables and hence provides a general response probability density function (PDF). In the second case, the input variable having the highest sensitivity index (in this case the TC/BC interface amplitude) has been fixed at its mean value ($A_{\text{mean}} = 20\mu m$) while the uncertainties in the rest of the input variables have been taken into account.

The probability density functions for both scenarios, which are obtained using the TBC lifetime responses from the surrogate model, are shown in Fig. 5b.

As may be observed from the figure, the PDF for a fixed interface amplitude of A_{mean} has approximately the shape of a normal distribution, whereas the PDF for an uncertain amplitude has a non-normal distribution with a significantly higher spread. It can also be observed that, if required for further processing, the PDF in the general case could be fitted to, for example, a Weibull distribution with suitable parameters. In order to further compare the degree of variance in the two above-mentioned scenarios, the coefficient of variation (COV) has been calculated for both cases by taking the ratio between the standard deviation and the mean value [25]. The COV for the first case (fixed interface amplitude) has been found out to be 45% whereas the second case (uncertain interface amplitude) has a COV of 22%. Since the TC/BC interface amplitude value is the most significant contributor to the output variance, controlling the TC/BC interface amplitude during manufacturing is beneficial in order to minimize the dispersion in the TBC lifetime and correspondingly increase the reliability of the TBC system.

4.5. Uncertainty propagation plots

To further visualize how the output changes while a particular input variable is controlled, the variation in TBC lifetime is plotted in Fig. 6 as a function of each random input variable ϕ_i while the uncertainties in the remaining input variables $\phi_{\sim i}$ are propagated through the surrogate model. The curves shown in Fig. 6 represent the trend of the response surface generated using the Wiener–Askey scheme of polynomials of order 2 for the considered PCE, and may not accurately predict certain non-linearities that tend to saturate. In particular, the results should be interpreted in terms of monotonic trends (increase or decrease of lifetime) whereas apparent local minimum values shown in Fig. 6 actually reflect slow changes in lifetime.

4.5.1. Uncertainty propagation of microstructural features

It can be observed from Fig. 6a that the TBC lifetime varies the most with changes in the TC/BC interface amplitude A. A decrease in the interface amplitude value leads to a gain in TBC lifetime. This observation has also been made by several researchers who have carried out two-dimensional as well as three dimensional finite element studies to understand the impact of roughness or the

TC/BC interface topography on damage growth and lifetime of TBCs. Specifically, studies have indicated that an increase in the value of interfacial waviness or roughness leads to increased magnitude of stresses at the TC/TGO and TGO/BC interfaces as well as the TC layer, thus affecting the fatigue life of TBCs [55,56]. It has also been observed that the development of damage as a result of thermal cycling is directly proportional to the interface roughness values [57]. This implies that in order to predict the TBC lifetime, special efforts need to be taken while measuring the value of interface amplitude. Additionally, focus should be given upon controlling the feedstock powder size during manufacturing of TBCs to obtain a desirable value of interface amplitude.

The variation of TBC lifetime with the TGO growth coefficient c shown in Fig. 6b indicates that the expected value of TBC lifetime reduces with an increase in the TGO growth coefficient value. This result agrees with the experimental and numerical investigations that indicate the effects of TGO thickness values on stress redistribution and damage growth in TBCs [46,58,59]. Thus, efforts can be implemented in order to reduce the TGO growth rate. It has been observed that the TGO growth rate can be controlled by modifying the BC manufacturing process [60] or by carrying out a pretreatment of the BC, which constrains the initiation and growth of cracks between the TC and TGO layers [61].

4.5.2. Uncertainty propagation of self-healing design

Regarding the design input variables for a self-healing system, it can be observed from Figs. 6c,d,e that there exists less variation in TBC lifetime across the considered ranges of healing particle volume fraction, particle diameter and the particle mean distance from TC/BC interface, respectively. In general, the lifetime slightly increases with increased volume fraction of healing particles, it tends to slightly decrease with increasing healing particle diameter and it tends to be insensitive to the average distance of the healing particles to the TC/BC interface, albeit within the range considered. This indicates that for the considered ranges of the design variables associated with healing particles, controlling the manufacturing process may not yield significant changes in the prediction of the TBC lifetime. However, the sensitivity analysis does not provide information regarding the effectiveness of the self-healing mechanism in terms of *extending* the lifetime of a TBC system, which is a critical technological question and it is addressed in the next section.
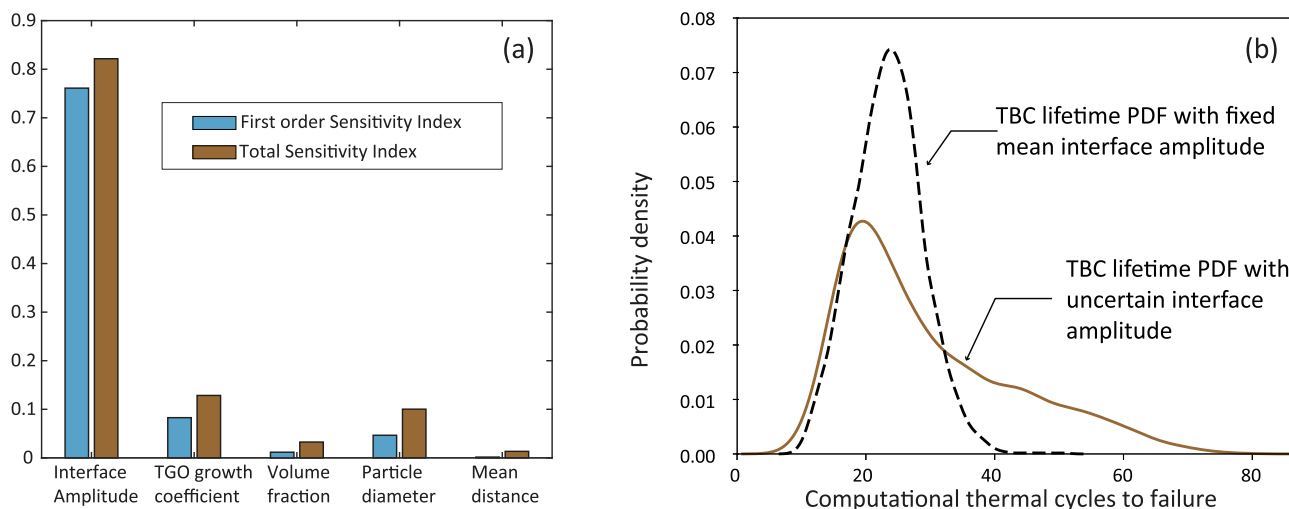

Fig. 5. (a): Indices depicting first-order and total sensitivity of self-healing TBC lifetime to the random input variables. (b): Lifetime PDF of a SH-TBC and effect on the PDF by fixing the input variable with the highest sensitivity index (TC/BC interface amplitude).
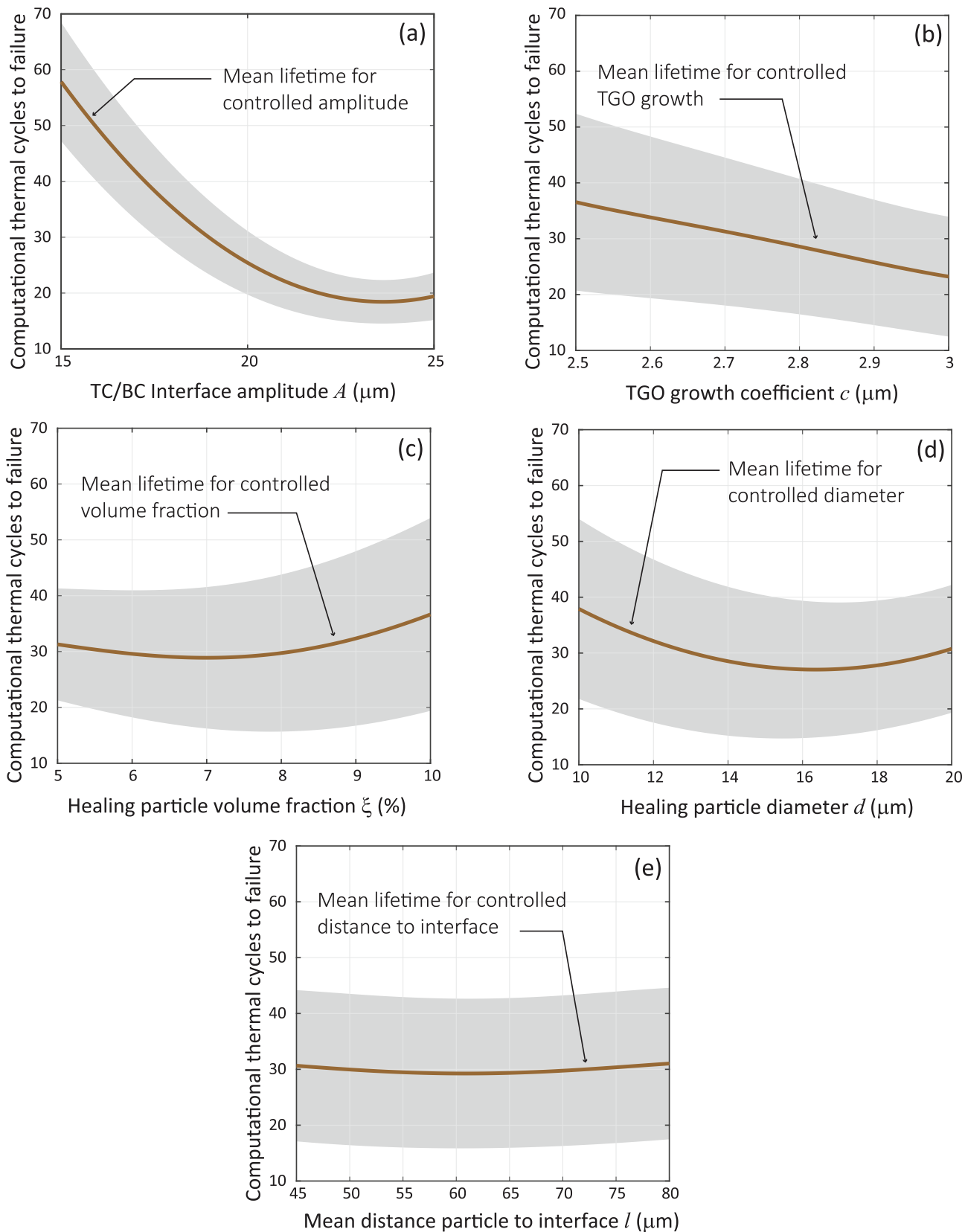
Fig. 6. Predicted TBC lifetime as a function of the parameter indicated on the horizontal axis, while propagating the uncertainties in the remaining parameters. Figures (a) through (e) correspond to the input variables indicated in Table 1, respectively. The gray region above and below the mean lifetime value corresponds to ± one sta.ndard deviation.

5. Uncertainty quantification of benchmark TBC lifetime and self-healing crack growth rate

5.1. Comparison with the benchmark TBC

In order to estimate how the use of self-healing particles in TBCs affects the expected lifetime and the underlying scatter as compared with the case of the conventional TBC without any healing particles, a separate PCE based surrogate model is developed for the conventional (benchmark) system with the same procedure as described in Fig. 2. This surrogate model considers the TC/BC interface amplitude and TGO growth rate as the input uncertain variables which are defined over the same respective distributions as that in the surrogate model developed for the self-healing TBC. In this case, $K = 2$ input random variables are used and, choosing an oversampling ratio of $n_p = 2$ and a polynomial order $n = 2$, there are $N = 12$ sample points required (see Table 2). Applying the same procedure as for the self-healing TBC, the surrogate model for the lifetime of the benchmark system is

$$L_{TBC} = 215.42 - 7.94A + 0.11A^2 + 0.61Ac - 77.40c + 11.65c^2. \tag{19}$$

In the above equation, L_{TBC} represents the lifetime of the benchmark TBC in number of computational thermal cycles as a function of the TC/BC interface amplitude A and the TGO growth rate coefficient c. The same characteristics for A and c are chosen as indicated in Table 1.

Similar to the surrogate model for the self-healing TBC, the model's goodness of fit and its predictive performance are evaluated computing the adjusted coefficient of determination and leave-one-out cross validation error, which in this case are given by $R^2_{A,TBC} = 0.99$ and $e_{L,TBC} = 0.91$, thus confirming that the surrogate model is able to capture reasonably well the predictions of the complex simulator.

The trained surrogate model L_{TBC} in (19) is utilized to acquire the distribution of lifetime for the benchmark TBC. The so-called box plots using the lifetime realizations of the surrogate models for the benchmark and self-healing TBC cases are shown in Fig. 7. As indicated in the figure, the surrogate model for the benchmark case provides a mean lifetime value of 13 computational thermal cycles while describing a coefficient of variation (COV) of 35%. On the other hand, the surrogate model for the self-healing TBC depicts a mean lifetime value of 29 computational thermal cycles and a COV = 45%. This indicates that for the considered range of values of the input variables, the use of self-healing particles helps to improve the expected TBC lifetime value but at the same time leads to increased scatter in the thermal fatigue life as compared with the benchmark TBC without any healing particles. This observation regarding the increased scatter in lifetime could potentially be attributed to the random distribution and inherent variations in the individual positions of the healing sites within the self-healing TBC. Additionally, the coupled effects of the considered input variables might affect the TBC lifetime, thus contributing to the scatter.
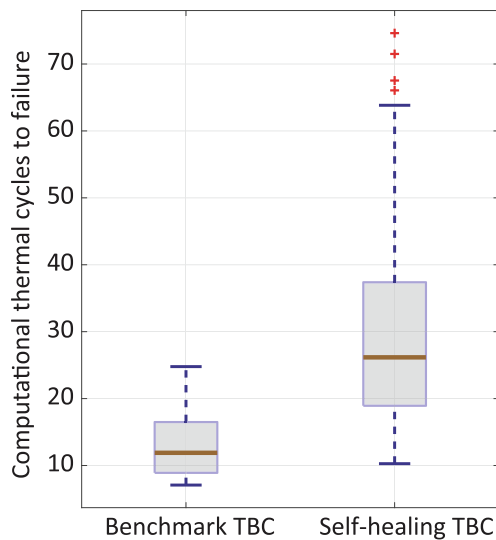
5.2. Uncertainty quantification of the self-healing TBC crack growth rate

In addition to the surrogate model for the lifetime of a self-healing TBC system, it is useful to develop alternative damage indicators for progressive failure. In particular, crack growth rates can be used to estimate the remaining lifetime of a system. To this end,
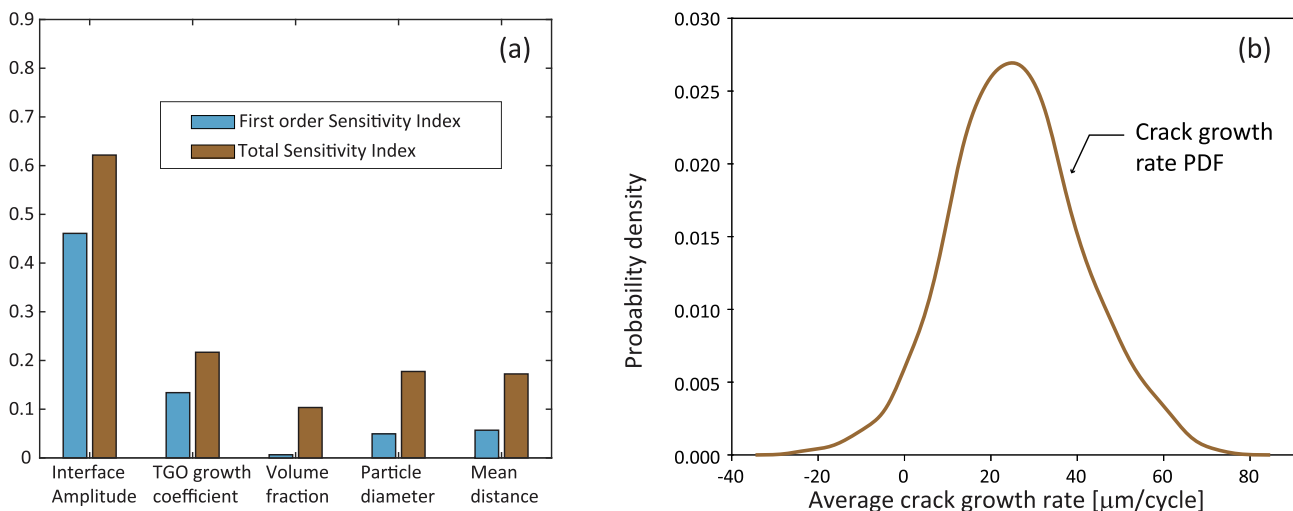

Fig. 7. Box plot comparison of the lifetime realizations for the benchmark TBC surrogate model (no-healing) and the self-healing TBC surrogate models.

Fig. 8. (a): Indices depicting first-order and total sensitivity of self-healing TBC average cyclic crack growth to the random input variables. (b): PDF of normalized average crack growth in a SH-TBC system (negative values correspond to healing).

a surrogate model for the *average growth rate of damage* in self-healing TBCs can be developed for the same random input variables as indicated in Table 1. This quantity measures the effective crack growth, which accounts for cracking (positive crack growth) and healing (negative crack growth). The growth rate, which is mainly due to horizontal cracks, should be normalized by the width of the computational domain (in the current simulations $w = 480 \mu$m) due to the horizontal periodicity of the boundary conditions.

The surrogate model for average crack growth, not shown here for conciseness, has a coefficient of determination of $R^2 = 0.91$ and a modified coefficient of determination of $R_A^2 = 0.82$. The sensitivity indices and the PDF of the surrogate model for crack growth are shown in Figs. 8a and 8b, respectively.

It can be observed from Fig. 8a that, similar to the previously found results for lifetime, the interface amplitude is the main contributor towards the variance in TBC crack growth rate. However, its relative importance is smaller for crack growth than for lifetime. In this case, the TGO growth coefficient and the self-healing parameters exhibit a higher influence, particularly for the total sensitivity index. This indicates that the self-healing variables act in a coupled manner towards the variance of the average crack growth. The probability density function for crack growth shown in Fig. 8b exhibits an approximately normal shape with a mean around 0.05 per cycle.

6. Conclusions

Surrogate modeling techniques provide an efficient way of approximating complex and deterministic numerical frameworks. These models are able to take into account the uncertainties in the input variables that are used to design the underlying framework in order to deliver reliable and computationally inexpensive results. From the surrogate model for self-healing TBCs the main findings are:

- The TC/BC interface amplitude is the most significant contributor towards the variance in TBC lifetime. This implies that relatively small changes in the value of the interface amplitude will result in large deviations in the lifetime. As a result, this calls for special efforts to determine the TC/BC interface amplitude value.
- The variables associated with healing particles have been found to demonstrate relatively minor influence towards the variation in TBC lifetime.
- The uncertainty propagation plots indicate that the expected TBC lifetime reduces with an increase in the TC/BC interface amplitude and TGO growth rate values. Therefore, in order to increase the TBC lifetime, caution should be exercised during the manufacturing of self-healing TBCs in the form of a control of the powder size and bond coat processing techniques.
- The incorporation of healing particles helps in improving the expected value of the TBC lifetime. However, it also leads to an increased amount of scatter in the thermal fatigue life as compared with that of the benchmark or the TBC model without any healing particles.
- Variables associated with self-healing particles seem to act in a coupled manner in order to contribute towards the variance in crack growth rate, albeit their overall contribution is minor.

The current research illustrates the benefits of an additional layer of analysis over the conventional deterministic approaches in order to estimate the reliability of the results and draw informed conclusions for the design of self-healing materials.

Data availability

The raw/processed data required to reproduce these findings cannot be shared at this time due to technical or time limitations.

Declaration of Competing Interest

The authors declare that they have no known competing financial interests or personal relationships that could have appeared to influence the work reported in this paper.

References

[1] J.G. Thakare, C. Pandey, M.M. Mahapatra, R.S. Mulik, Thermal barrier coatings—a state of the art review, Met. Mater. Int. 27 (7) (2020) 1947–1968, https://doi.org/10.1007/s12540-020-00705-w.

[2] G. Mehboob, M.-J. Liu, T. Xu, S. Hussain, G. Mehboob, A. Tahir, A review on failure mechanism of thermal barrier coatings and strategies to extend their lifetime, Ceram. Int. 46 (7) (2020) 8497–8521, https://doi.org/10.1016/j.ceramint.2019.12.200.

[3] A.L. Carabat, M.J. Meijerink, J.C. Brouwer, E.M. Kelder, J.R. van Ommen, S. van der Zwaag, W.G. Sloof, Protecting the MoSi₂ healing particles for thermal barrier coatings using a sol-gel produced Al₂O₃ coating, J. Eur. Ceram. Soc. 38 (7) (2018) 2728–2734, https://doi.org/10.1016/j.jeurceramsoc.2018.02.002.

[4] Y. Chen, X. Zhang, S. van der Zwaag, W.G. Sloof, P. Xiao, Damage evolution in a self-healing air plasma sprayed thermal barrier coating containing self-shielding MoSi_2 particles, J. Am. Ceram. Soc. 102 (8) (2019) 4899–4910, https://doi.org/10.1111/jace.16313.

[5] J. Krishnasamy, S.A. Ponnusami, S. Turteltaub, S. van der Zwaag, Thermal cyclic behavior and lifetime prediction of self-healing thermal barrier coatings, Int. J. Solids Struct. 222–223 (2021) 111034, https://doi.org/10.1016/j.ijsolstr.2021.03.021.

[6] W.G. Sloof, S. Turteltaub, A. Carabat, Z. Derelioglu, S. Ponnusami, G. Song, Crack healing in yttria stabilized zirconia thermal barrier coatings, Self Healing Materials: Pioneering Research in the Netherlands 219.

[7] J. Krishnasamy, S.A. Ponnusami, S. Turteltaub, S. van der Zwaag, Numerical investigation into the effect of splats and pores on the thermal fracture of air plasma-sprayed thermal barrier coatings, J. Therm. Spray Technol. 28 (8) (2019) 1881–1892, https://doi.org/10.1007/s11666-019-00949-y.

[8] J. Krishnasamy, S.A. Ponnusami, S. Turteltaub, S. van der Zwaag, Computational investigation of porosity effects on fracture behavior of thermal barrier coatings, Ceram. Int. 45 (16) (2019) 20518–20527, https://doi.org/10.1016/j.ceramint.2019.07.031.

[9] J. Krishnasamy, S.A. Ponnusami, S. Turteltaub, S. van der Zwaag, Modelling the fracture behaviour of thermal barrier coatings containing healing particles, Mater. Des. 157 (2018) 75–86, https://doi.org/10.1016/j.matdes.2018.07.026.

[10] S.A. Ponnusami, J. Krishnasamy, S. Turteltaub, S. van der Zwaag, A micromechanical fracture analysis to investigate the effect of healing particles on the overall mechanical response of a self-healing particulate composite, Fatigue Fract. Eng. Mater. Struct. 42 (2) (2018) 533–545, https://doi.org/10.1111/ffe.12929.

[11] S.A. Ponnusami, S. Turteltaub, S. van der Zwaag, Cohesive-zone modelling of crack nucleation and propagation in particulate composites, Eng. Fract. Mech. 149 (2015) 170–190, https://doi.org/10.1016/j.engfracmech.2015.09.050.

[12] L. Zhang, Y. Wang, W. Fan, Y. Gao, Y. Sun, Y. Bai, A simulation study on the crack propagation behavior of nanostructured thermal barrier coatings with tailored microstructure, Coatings 10 (8) (2020) 722, https://doi.org/10.3390/coatings10080722.

[13] S.M. Bostancı, E. Gürses, D. Çöker, Finite element modelling of TBC failure mechanisms by using XFEM and CZM, Procedia Structural Integrity 21 (2019) 91–100, https://doi.org/10.1016/j.prostr.2019.12.090.

[14] J. Song, S. Li, X. Yang, D. Shi, H. Qi, Numerical study on the competitive cracking behavior in TC and interface for thermal barrier coatings under thermal cycle fatigue loading, Surf. Coat. Technol. 358 (2019) 850–857, https://doi.org/10.1016/j.surfcoat.2018.11.006.

[15] L.-S. Wang, Z.-Y. Wei, B. Cheng, M.-J. Liu, G.-R. Li, H. Dong, G.-J. Yang, Gradient stiffening induced interfacial cracking and strain tolerant design in thermal barrier coatings, Ceram. Int. 46 (2) (2020) 2355–2364, https://doi.org/10.1016/j.ceramint.2019.09.226.

[16] Z.-Y. Wei, H.-N. Cai, Comprehensive effects of TGO growth on the stress characteristic and delamination mechanism in lamellar structured thermal barrier coatings, Ceram. Int. 46 (2) (2020) 2220–2237, https://doi.org/10.1016/j.ceramint.2019.09.207.

[17] X. Fan, R. Xu, T.J. Wang, Interfacial delamination of double-ceramic-layer thermal barrier coating system, Ceram. Int. 40 (9) (2014) 13793–13802, https://doi.org/10.1016/j.ceramint.2014.05.095.

[18] L. Wang, D.C. Li, J.S. Yang, F. Shao, X.H. Zhong, H.Y. Zhao, K. Yang, S.Y. Tao, Y. Wang, Modeling of thermal properties and failure of thermal barrier coatings with the use of finite element methods: A review, J. Eur. Ceram. Soc. 36 (6) (2016) 1313–1331, https://doi.org/10.1016/j.jeurceramsoc.2015.12.038.

[19] T.S. Hille, T.J. Nijdam, A.S.J. Suiker, S. Turteltaub, W.G. Sloof, Damage growth triggered by interface irregularities in thermal barrier coatings, Acta Mater. 57 (9) (2009) 2624–2630, https://doi.org/10.1016/j.actamat.2009.01.022.

[20] A.-S. Farle, J. Krishnasamy, S. Turteltaub, C. Kwakernaak, S. van der Zwaag, W. G. Sloof, Determination of fracture strength and fracture energy of (metallo-) ceramics by a wedge loading methodology and corresponding cohesive zone-based finite element analysis, Eng. Fract. Mech. 196 (2018) 56–70, https://doi.org/10.1016/j.engfracmech.2018.03.014.

[21] P. Honarmandi, R. Arróyave, Uncertainty quantification and propagation in computational materials science and simulation-assisted materials design, Integrating Materials and Manufacturing Innovation 9 (1) (2020) 103–143, https://doi.org/10.1007/s40192-020-00168-2.

[22] S. Dutta, A.H. Gandomi, Design of experiments for uncertainty quantification based on polynomial chaos expansion metamodels, in: Handbook of Probabilistic Models, Elsevier, 2020, pp. 369–381. doi:10.1016/b978-0-12-816514-0.00015-1.

[23] L.L. Gratiet, S. Marelli, B. Sudret, Metamodel-based sensitivity analysis: Polynomial chaos expansions and gaussian processes, in: Handbook of Uncertainty Quantification, Springer International Publishing, 2017, pp. 1289–1325. doi:10.1007/978-3-319-12385-1_38.

[24] C. Soize, R. Ghanem, Physical systems with random uncertainties: Chaos representations with arbitrary probability measure, SIAM Journal on Scientific Computing 26 (2) (2004) 395–410, https://doi.org/10.1137/s1064827503424505.

[25] K.M. Hamdia, M. Silani, X. Zhuang, P. He, T. Rabczuk, Stochastic analysis of the fracture toughness of polymeric nanoparticle composites using polynomial chaos expansions, Int. J. Fract. 206 (2) (2017) 215–227, https://doi.org/10.1007/s10704-017-0210-6.

[26] D. Kumar, Y. Koutsawa, G. Rauchs, M. Marchi, C. Kavka, S. Belouettar, Efficient uncertainty quantification and management in the early stage design of composite applications, Compos. Struct. 251 (2020) 112538, https://doi.org/10.1016/j.compstruct.2020.112538.

[27] M. Pathan, S. Ponnusami, J. Pathan, R. Pitisongsawat, B. Erice, N. Petrinic, V. Tagarielli, Predictions of the mechanical properties of unidirectional fibre composites by supervised machine learning, Scientific reports 9 (1) (2019) 1–10.

[28] R.H. Lopez, C.R.Á. da Silva, A non-intrusive methodology for the representation of crack growth stochastic processes, Mech. Res. Commun. 64 (2015) 23–28, https://doi.org/10.1016/j.mechrescom.2014.12.005.

[29] A.T. Beck, W.J. de Santana Gomes, Stochastic fracture mechanics using polynomial chaos, Probab. Eng. Mech. 34 (2013) 26–39, https://doi.org/10.1016/j.probengmech.2013.04.002.

[30] S. Yang, F. Xiong, F. Wang, Polynomial chaos expansion for probabilistic uncertainty propagation, in: Uncertainty Quantification and Model Calibration, InTech, 2017. doi:10.5772/intechopen.68484.

[31] B. Bhattacharyya, A critical appraisal of design of experiments for uncertainty quantification, Archives of Computational Methods in Engineering 25 (3) (2017) 727–751, https://doi.org/10.1007/s11831-017-9211-x.

[32] S.-K. Choi, R.V. Grandhi, R.A. Canfield, C.L. Pettit, Polynomial chaos expansion with latin hypercube sampling for estimating response variability, AIAA Journal 42 (6) (2004) 1191–1198, https://doi.org/10.2514/1.2220.

[33] S. Hosder, R. Walters, M. Balch, Efficient sampling for non-intrusive polynomial chaos applications with multiple uncertain input variables, in: 48th AIAA/ASME/ASCE/AHS/ASC Structures, Structural Dynamics, and Materials Conference, American Institute of Aeronautics and Astronautics, 2007. doi:10.2514/6.2007-1939.

[34] B. Sudret, S. Marelli, J. Wiart, Surrogate models for uncertainty quantification: An overview, in: 2017 11th European Conference on Antennas and Propagation (EUCAP), IEEE, 2017. doi:10.23919/eucap.2017.7928679.

[35] R. Eriksson, S. Sjöström, H. Brodin, S. Johansson, L. Östergren, X.-H. Li, TBC bond coat–top coat interface roughness: Influence on fatigue life and modelling aspects, Surf. Coat. Technol. 236 (2013) 230–238, https://doi.org/10.1016/j.surfcoat.2013.09.051.

[36] J.P. Martins, Y. Chen, G. Brewster, R. McIntyre, P. Xiao, Investigation of the bond coat interface topography effect on lifetime, microstructure and mechanical properties of air-plasma sprayed thermal barrier coatings, J. Eur. Ceram. Soc. 40 (15) (2020) 5719–5730, https://doi.org/10.1016/j.jeurceramsoc.2020.05.082.

[37] J. Jiang, B. Xu, W. Wang, R.A. Adjei, X. Zhao, Y. Liu, Finite element analysis of the effects of thermally grown oxide thickness and interface asperity on the cracking behavior between the thermally grown oxide and the bond coat, Journal of Engineering for Gas Turbines and Power 139 (2). doi:10.1115/1.4034259.

[38] T. Beck, R. Herzog, O. Trunova, M. Offermann, R.W. Steinbrech, L. Singheiser, Damage mechanisms and lifetime behavior of plasma-sprayed thermal barrier

[39] T.S. Hille, S. Turteltaub, A.S.J. Suiker, Oxide growth and damage evolution in thermal barrier coatings, Eng. Fract. Mech. 78 (10) (2011) 2139–2152, https://doi.org/10.1016/j.engfracmech.2011.04.003.

[40] Q.Q. Zhou, L. Yang, C. Luo, F.W. Chen, Y.C. Zhou, Y.G. Wei, Thermal barrier coatings failure mechanism during the interfacial oxidation process under the interaction between interface by cohesive zone model and brittle fracture by phase-field, Int. J. Solids Struct. 214 (2021) 18–34, https://doi.org/10.1016/j.ijsolstr.2020.12.020.

[41] T.H. Nguyen, K. Chang, Comparison of the point-collocation non-intrusive polynomial (NIPC) and non-intrusive spectral projection (NISP) methods for the γ-r$_\theta$ transition model, Applied Sciences 9 (7) (2019) 1407, https://doi.org/10.3390/app9071407.

[42] B. Sudret, M. Berveiller, M. Lemaire, A stochastic finite element procedure for moment and reliability analysis, European Journal of Computational Mechanics 15 (7–8) (2006) 825–866, https://doi.org/10.3166/remn.15.825-866.

[43] J. Feinberg, H.P. Langtangen, Chaospy: An open source tool for designing methods of uncertainty quantification, Journal of Computational Science 11 (2015) 46–57, https://doi.org/10.1016/j.jocs.2015.08.008.

[44] C. Geuzaine, J.-F. Remacle, Gmsh: A 3-d finite element mesh generator with built-in pre- and post-processing facilities, Int. J. Numer. Meth. Eng. 79 (11) (2009) 1309–1331, https://doi.org/10.1002/nme.2579.

[45] S.A. Ponnusami, J. Krishnasamy, S. Turteltaub, S. van der Zwaag, A cohesive-zone crack healing model for self-healing materials, Int. J. Solids Struct. 134 (2018) 249–263, https://doi.org/10.1016/j.ijsolstr.2017.11.004.

[46] L. Lim, S. Meguid, Temperature dependent dynamic growth of thermally grown oxide in thermal barrier coatings, Materials & Design 164 (2019) 107543, https://doi.org/10.1016/j.matdes.2018.107543.

[47] Z.-Y. Wei, H.-N. Cai, Comprehensive effects of TGO growth on the stress characteristic and delamination mechanism in lamellar structured thermal barrier coatings, Ceram. Int. 46 (2) (2020) 2220–2237, https://doi.org/10.1016/j.ceramint.2019.09.207.

[48] Q. Shen, L. Yang, Y. Zhou, Y. Wei, N. Wang, Models for predicting TGO growth to rough interface in TBCs, Surf. Coat. Technol. 325 (2017) 219–228, https://doi.org/10.1016/j.surfcoat.2017.06.001.

[49] D. Xiu, G.E. Karniadakis, The Wiener-Askey polynomial chaos for stochastic differential equations, SIAM Journal on Scientific Computing 24 (2) (2002) 619–644, https://doi.org/10.1137/s1064827501387826.

[50] B. Sudret, Global sensitivity analysis using polynomial chaos expansions, Reliability Engineering & System Safety 93 (7) (2008) 964–979, https://doi.org/10.1016/j.ress.2007.04.002.

[51] M.S. Alam, N. Sultana, S.Z. Hossain, Bayesian optimization algorithm based support vector regression analysis for estimation of shear capacity of FRP reinforced concrete members, Applied Soft Computing 105 (2021) 107281, https://doi.org/10.1016/j.asoc.2021.107281.

[52] Q. Hu, Q. Huang, D. Yang, H. Liu, Prediction of breakthrough curves in a fixed-bed column based on normalized gudermannian and error functions, J. Mol. Liq. 323 (2021) 115061, https://doi.org/10.1016/j.molliq.2020.115061.

[53] G. Blatman, B. Sudret, Adaptive sparse polynomial chaos expansion based on least angle regression, J. Comput. Phys. 230 (6) (2011) 2345–2367, https://doi.org/10.1016/j.jcp.2010.12.021.

[54] G. Blatman, B. Sudret, Efficient computation of global sensitivity indices using sparse polynomial chaos expansions, Reliability Engineering & System Safety 95 (11) (2010) 1216–1229, https://doi.org/10.1016/j.ress.2010.06.015.

[55] E. Busso, Z. Qian, M. Taylor, H. Evans, The influence of bondcoat and topcoat mechanical properties on stress development in thermal barrier coating systems, Acta Mater. 57 (8) (2009) 2349–2361, https://doi.org/10.1016/j.actamat.2009.01.017.

[56] P. Skalka, K. Sláme čka, J. Pokluda, L. Čelko, Stability of plasma-sprayed thermal barrier coatings: The role of the waviness of the bond coat and the thickness of the thermally grown oxide layer, Surf. Coat. Technol. 274 (2015) 26–36, https://doi.org/10.1016/j.surfcoat.2015.04.021.

[57] L. Saucedo-Mora, K. Sláme čka, U. Thandavamoorthy, T. Marrow, Multi-scale modeling of damage development in a thermal barrier coating, Surf. Coat. Technol. 276 (2015) 399–407, https://doi.org/10.1016/j.surfcoat.2015.06.038.

[58] J. Jiang, W. Wang, X. Zhao, Y. Liu, Z. Cao, P. Xiao, Numerical analyses of the residual stress and top coat cracking behavior in thermal barrier coatings under cyclic thermal loading, Eng. Fract. Mech. 196 (2018) 191–205, https://doi.org/10.1016/j.engfracmech.2018.04.031.

[59] T.S. Hille, S. Turteltaub, A.S.J. Suiker, Oxide growth and damage evolution in thermal barrier coatings, Eng. Fract. Mech. 78 (10) (2011) 2139–2152, https://doi.org/10.1016/j.engfracmech.2011.04.003.

[60] K. Ogawa, A. Nakano, Thermally grown oxide growth behavior and its impedance properties of thermal barrier coatings with cold sprayed and low pressure plasma sprayed bond coatings, J. Soc. Mater. Sci., Japan 62 (2) (2013) 131–136, https://doi.org/10.2472/jsms.62.131.

[61] W. Chen, M. Liu, J. Zhang, Z. Deng, J. Mao, High-temperature oxidation behavior and analysis of impedance spectroscopy of 7YSZ thermal barrier coating prepared by plasma spray-physical vapor deposition, Chin. J. Aeronaut. 31 (8) (2018) 1764–1773, https://doi.org/10.1016/j.cja.2017.12.008.